DOE/ER52147-6

MICROWAVE GENERATION FOR MAGNETIC FUSION ENERGY APPLICATIONS

Progress Report

July 15, 1992 to July 14, 1993

Principal Investigators

T.M. Antonsen, Jr., W.W. Destler, V.L. Granatstein, and B. Levush

Laboratory for Plasma Research

and

Electrical Engineering Department

University of Maryland

College Park, MD 20742

February 1993

PREPARED FOR THE U.S. DEPARTMENT OF ENERGY UNDER
CONTRACT NUMBER DEFG05-87ER52147

PREFACE

This progress report encompasses work on two separate projects, both related to developing sources for electron cyclotron resonance heating of magnetic fusion plasmas. The report is therefore divided into two parts as follows:

Task A Free Electron Lasers with Small Period Wigglers

DOE/ER/52147--6

DE93 013864

Task B Theory and Modeling of High Frequency, High Power Gyrotron Operation

Task A is experimental and eventually aims at developing continuously tunable, cw sources for ECRH with power per unit as high as 5 megawatts. Task B provides gyrotron theory and modeling in support of the gyrotron development programs at MIT and Varian.

TASK A
FREE ELECTRON LASERS WITH SMALL PERIOD WIGGLERS

Contents

1 INTRODUCTION

At present the leading millimeter wave generator being developed for Electron Cyclotron Resonance (ECR) applications in the magnetic fusion program is the fixed frequency gyrotron oscillator. The focus of gyrotron research is achieving 1 MW cw output power [1-3]; the potential for stepwise frequency tunability of a gyrotron by mode switching has also received attention [1,4]. Free Electron Laser (FEL) amplifiers may provide an attractive alternative as ECR sources since they have the potential of operating with cw power per amplifier much larger than 1 MW, and they would be continuously tunable.

Experiments at the Lawrence Livermore National Laboratory [5] have shown the feasibility of high pulsed power, high efficiency, millimeter-wave FEL amplifiers driven by electron beams of several MeV energy. Our work strives to develop high average power FELs at voltages below 1 MV allowing for smaller and less costly power supplies. To achieve operation of an FEL with 100 GHz $\lesssim f \lesssim$ 150 GHz and with relatively modest voltage, we have been investigating the use of small period ($\lambda_w \sim 1$ cm) planar wiggler magnets together with sheet electron beams. The sheet beam geometry allows for an FEL interaction region in the form of a narrow slit with high wiggler field at the center plane where the electrons are concentrated. The total current and power may then be increased without making current density excessive by increasing the wide dimension of the sheet beam. Sheet beam FEL design parameters for both a Proof-of-Principle (PoP) FEL experiment, which is current in progress, and an ITER relevant FEL design are shown in Table 1.

A central issue in the sheet beam FEL concept is propagation of the beam through the interaction region without excessive interception by the walls. In section 2 below we describe a successful experimental demonstration of sheet beam propagation through a 56 period uniform wiggler. Cold testing and initial hot test operation of the (PoP) FEL amplifier are also described. Finally, we present a theoretical investigation of the bandwidth of an FEL amplifier with a tapered wiggler operating in saturation.

Table 1: FEL amplifier design parameters. (Input rf power assumed to 1 kW.)

FEL Parameters	ITER Relevant Design	Proof-of-Principle Experiment
Frequency, f	150 GHz	94 GHz
Voltage, ϕ_{HV}	860 kV	470 kV
Current, I_b	30 A	10 A
Beam thickness, y_b	3 mm	1 mm
Beam width, x_b	3 cm	2 cm
Waveguide height, b	7.5 mm	3.2 mm
Waveguide width, a	4 cm	4 cm
Wiggler period, λ_w	1.5 cm	0.96 cm
Peak flux density (untapered wiggler), B_{w0}	7.0 kG	5.1 kG
Wiggler parameter, a_{w0}	0.98	0.46
Linear gain (untapered wiggler)	0.44 dB/cm	0.47 dB/cm
Length of untapered wiggler	63 cm	50 cm
Saturated power at end of untapered wiggler	620 kW	180 kW
Length of tapered wiggler	66 cm	54 cm
Output power	5 MW	0.4 MW
Intrinsic FEL efficiency	19%	8.5%
Maximum RF wall heating	1.1 kW/cm^2	
Total efficiency (with 80% energy recovery)	54%	
Main power supply voltage (with 80% energy recovery), ϕ_{LV}	309 kV	

2 TECHNICAL PROGRESS

2.1 Sheet Beam Propagation Studies

The configuration for the sheet beam amplifier experiment is shown in Fig. 1. The sheet beam is formed by explosive high-field emission of electrons from a cold cathode (component no. 7) and scrapping by a two slot anode (component no. 8). Initial beam propagation studies were carried out in the absence of both the miter bend (component no. 9) and the amplifier waveguide (component no. 11). In this case, after carefully adjusting the shape of the entrance magnetic field and instituting the offset pole technique to achieve focusing in the wiggler plane at the edges of the sheet, excellent beam propagation efficiency was achieved.

In Fig. 2 both the injected current measured directly behind the anode, and the current after passing through a 56 period wiggler magnet are plotted as a function of the width of the sheet beam. It is seen that for widths up to $\sim$ 20 mm almost complete beam transport is achieved, and that for a width of 20 mm a current of 14 A is propagated. In these measurements, the sheet beam thickness was 1.0 mm, and the beam channel transverse dimensions were 59 mm by 3.2 mm. The peak wiggler field was 5 kG, and the wiggler period was 9.6 mm. Electron energy was 470 keV.

Subsequent beam propagation experiments were in the presence of both the miter bend, which is required to launch the 94 GHz signal, and the amplifier waveguide, which is required to propagate the signal. The waveguide inner dimensions were 40 mm by 2.6 mm. About 90% of the injected current in a 20 mm $\times$ 1 mm sheet beam could be propagated through the waveguide when the peak wiggler field was 3 kG. However, only 50% propagation was achieved for a wiggler peak field of 4.8 kG. The reason for the reduced transport efficiency is certainly related to the reduced dimension of the amplifier waveguide compared with the channel dimensions in the absence of the waveguide.

The situation is further aggravated by the fact that as waveguide height becomes smaller, the cutoff frequency of the TE_{01} FEL mode rises and a larger value of electron energy is required to ensure resonance between the electron axial velocity and the phase velocity of the FEL pondermotive beat wave. (See Appendix I). In fact, for a waveguide height of 2.6 mm, the resonant energy is $\sim$760 keV. With this value of accelerating voltage only 35% of the incident beam could be injected through the wiggler magnet.

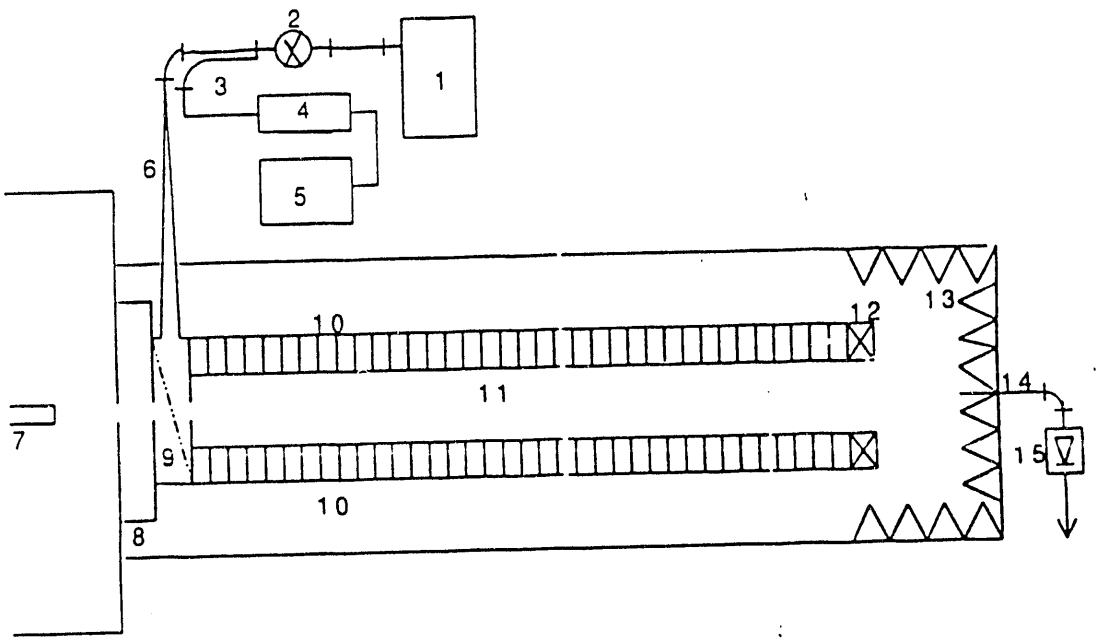

Figure 1: FEL amplifier experiment configuration: 1) EIO tube; 2) fixed attenuator, −20 dB; 3) directional coupler, −20 dB; 4) sensor; 5) power meter; 6) waveguide taper; 7) cathode; 8) two slot anode; 9) miter bend; 10) planar wiggler, 56 periods; 11) amplifier waveguide; 12) Rogowski coil; 13) absorption material; 14) waveguide antenna, w-band; 15) microwave diode.

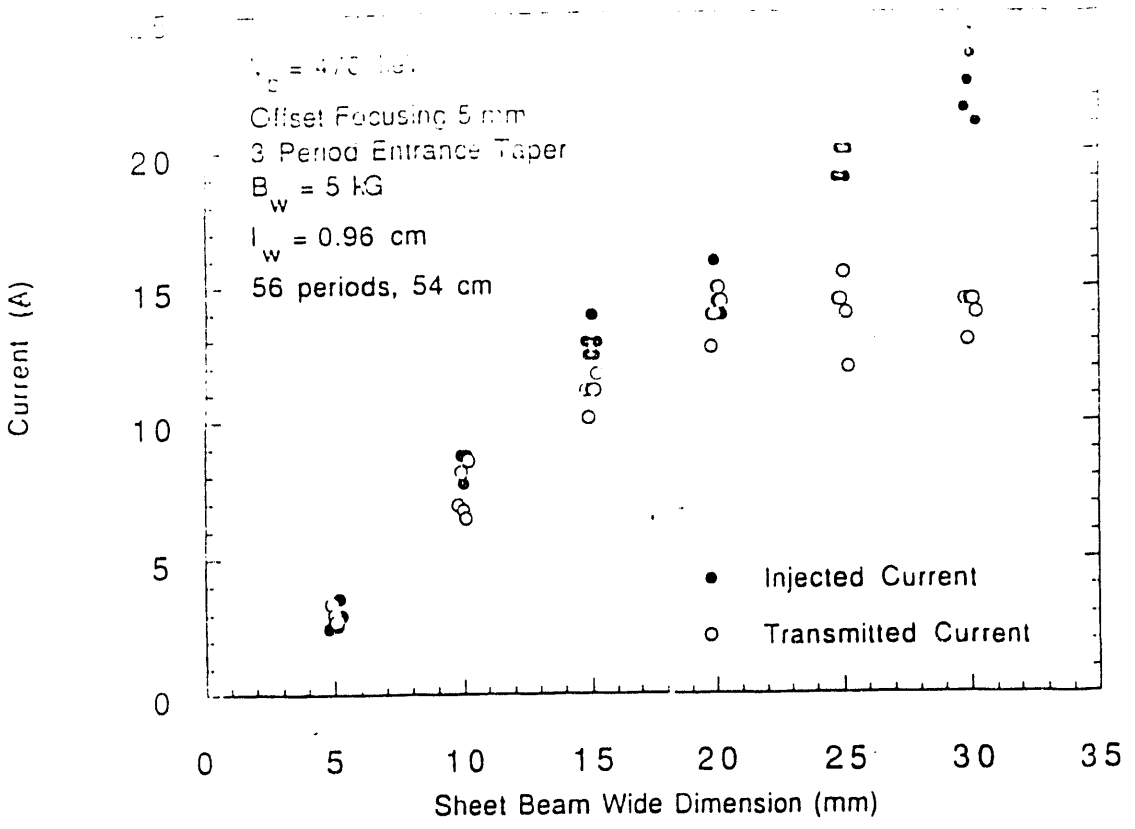

Figure 2: Beam propagation results.

2.2 Small Signal FEL Amplifier Studies

Cold testing of the entire FEL amplifier system as shown in Fig. 1 has been completed. This first required conditioning of the 94 GHz Extended Interaction Oscillator (EIO) (component no. 1 in Fig. 1). After conditioning, the EIO produced an output power of 10 W cw. The measured overall insertion loss for the EIO output waveguide through the waveguide taper (component no. 6), the miter bend (component no. 10) and the amplifier waveguide (component no. 11) was −2.5 dB. The waveguide taper is used to match the EIO output waveguide to the miter bend and accomplishes the required mode conversion. The miter bend itself is used as a beam-wave injection coupler.

A limited attempt (about 40 shots) to achieved FEL amplifier operation was carried out using the DRAGON pulse line accelerator. The beam energy required for FEL resonance was in the range 700-800 keV (see Appendix I), and DRAGON had to be operated in a mismatched state to achieve the required pulsed voltage. In this mismatched state, the velvet cathode was damaged about every five shots, and reproducibility was poor.

In three shots, there was an indication that microwave amplification had been achieved.

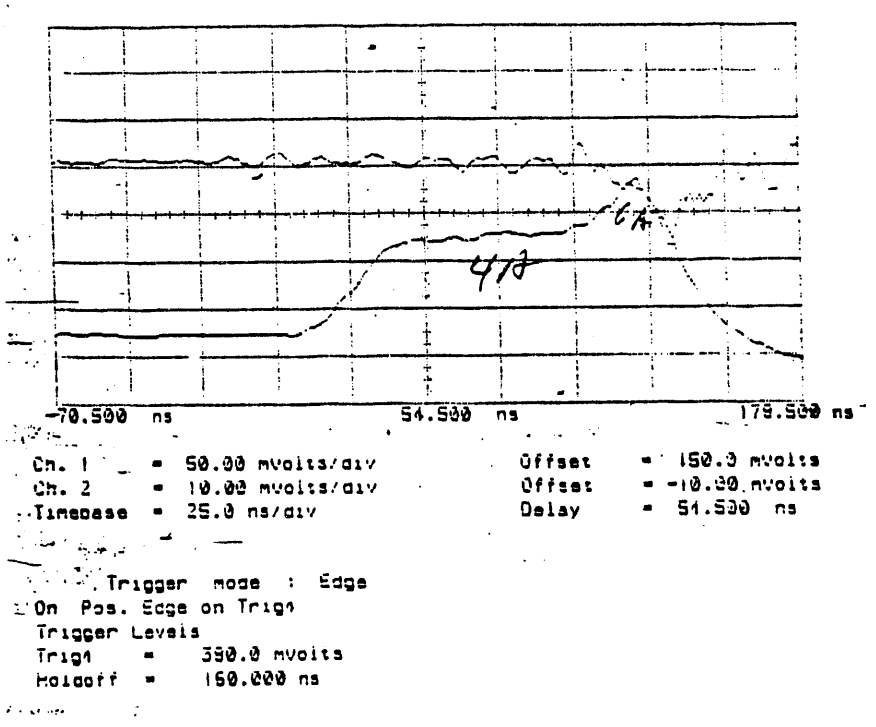

Figure 3: Traces of current propagated through the wiggler magnet (lower trace), and signal on the microwave diode detector (upper trace).

The operating parameter for these shots are is follows: beam current transported through the waveguide 6A, beam energy 763 keV, and peak wiggler magnetic field 4.8 kG. In Fig. 3, traces of the current propagated through the wiggler and the microwave detector signal are shown. The current rises from 4 amperes to 6 amperes toward the end of the pulse and the microwave diode signal appears when the current is maximum. The reproducibility of the experiment needs to be improved to increase confidence in this result and study it quantitatively.

2.3 Theoretical Studies of Tunability of a Tapered FEL Amplifier

Tapering the strength of the wiggler field or tapering the period of the wiggler is a way to achieve high efficiency operation for the FEL amplifier. The tapering is designed to maximize the number of trapped particles at saturation and to minimize the detrapping processes as the particles are further slowing down before exiting the interaction region. The design of the taper is made for a particular frequency of operation. The question is how the efficiency

of a tapered FEL amplifier will change when a wave at a different frequency is injected. To address this question we optimized the tapering of the wiggler period for an FEL amplifier at 94 GHz. The design parameters of such an FEL are shown in Fig. 4. We found that the efficiency of the interaction is not sensitive to the frequency of FEL operation. We varied the injected frequency from 75 GHz to 110 GHz, while the efficiency changed only from 29% to 22% (see Fig. 5). For each frequency we found the optimum injected beam energy (see Fig. 6).

This study has been performed using our 1-D FEL amplifier code. Presently, we are in the process of performing similar simulations with more realistic 3-D FEL amplifier code. Preliminary results from this study confirm our 1-D simulation results. This work is being done in collaboration with Dr. H. Freund.

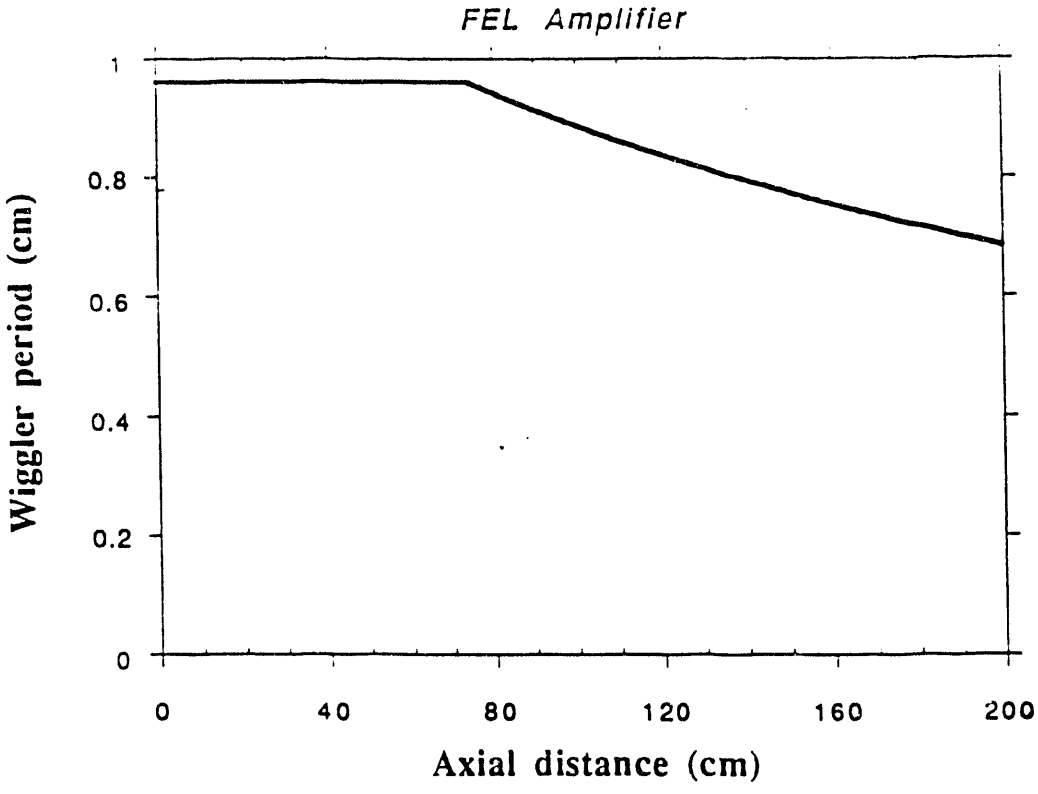

the length of the straight section	*74 (cm)*
total length	*200 (cm)*
wiggler period in the straight section	*0.96 (cm)*
wiggler period at the exit	*0.68 (cm)*
wiggler strength in the straight section	*5.1 (kG)*
input power	*1 (kW)*

Figure 4: Tunability of tapered FEL amplifier. Wiggler period tapering designed for 94 GHz.

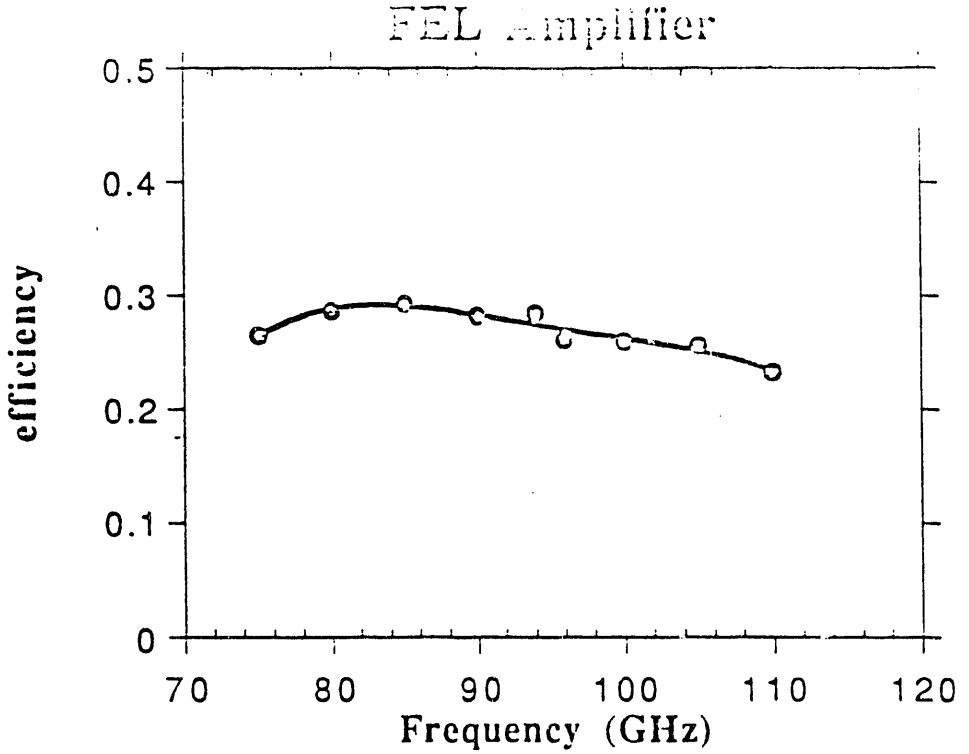

Figure 5:

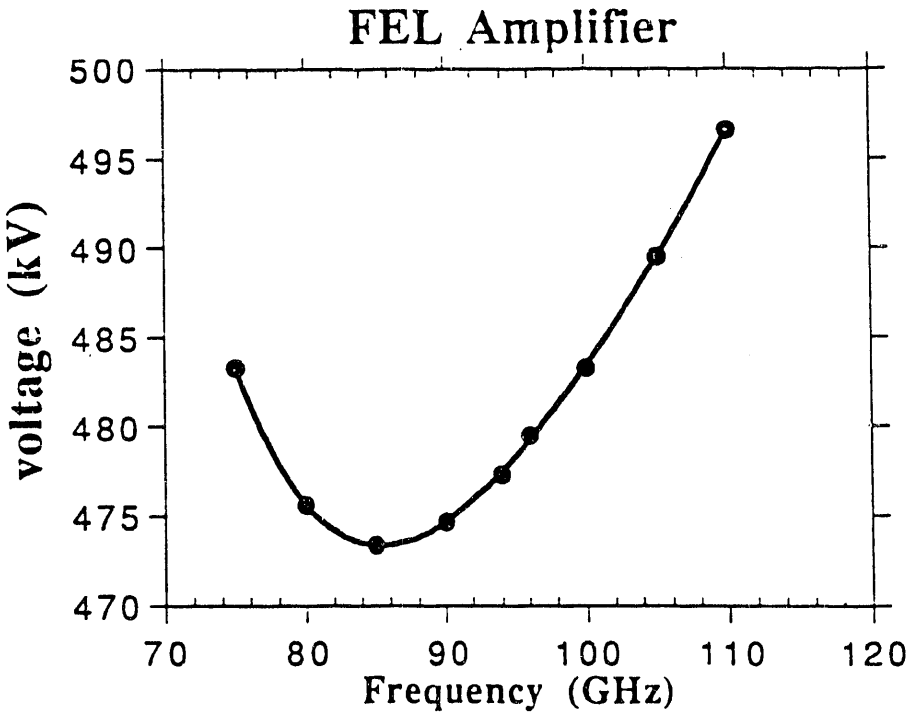

Figure 6:

REFERENCES

1. K.L. Kreischer and R.J. Temkin, Phys. Rev. Lett. **59** (1987) 547.

2. K. Felch, C. Hess, M. Huey, E. Jongewaard, H. Jory, J. Nielson, R. Pendleton, and M. Tsirulnikov, Proc. SPIE **1514** (1990) 315.

3. V.A. Flyagin and G.S. Nusinovich, Proc. IEEE **76** (1988) 644.

4. G.G. Denisov, M.I. Petelin, M. Yu. Shmelyov, I.N. Treskin, D.V. Vinogradov, and V.E. Zepavalov, "Frequency-tunable gyrotron," Report no. ITER-IL-HD-6-0-21, ITER Team, Max-Planck-Institut für Plasmaphysik, D8046, Garching, Germany, 1989.

5. T.J. Orzechowski, B.R. Anderson, J.C. Clark, W.M. Fawley, A.C. Paul, D. Prosnitz, E.T. Scharlemann, S.M. Yarema, D.B. Hopkins, A.M. Sessler, and J.S, Wurtele, Phys. Rev. Lett. **57** (1986) 2172.

3 TASK A PUBLICATIONS

Copies of these papers can be found in Appendix A2.

1. V.L. Granatstein, W.W. Destler, S.W. Bidwell, Z.X. Zhang, T.M. Antonsen, Jr., B. Levush, J. Rodgers, Y. Carmel, and H. Freund, "Experimental and Numerical Results on a Millimeter-Wave Free Electron laser Amplifier," 1992 FEL Conference, Kobe, Japan.

2. Z.X. Zhang, V.L. Granatstein, W.W. Destler, S.W. Bidwell, and J. Rodgers, "Experimental and Numerical Studies of Sheet Electron Beam Propagation through a Planar Wiggler Magnet," to be submitted to J. of Appl. Phys.

Reprints + Preprints removed

4 STATEMENT OF WORK (July 15, 1993-July 14, 1994)

4.1 Completion of Small Signal Amplification Studies

The wiggler magnet will be reconfigured and improved by the used of magnetic material with properties superior to iron. This will allow for achieving the required 5 kG field at the location of the sheet electron beam while making the gap in the magnet significantly larger. If the height of the waveguide can be made with an inside dimension of 3.2 mm the resonant electron energy is then ~470 keV. This value of energy is much more compatible with reliable and reproducible operation of available equipment, and will also have advantages in the eventual amplifier parameters. After improving the magnet the small signal studies of the 94 GHz FEL amplifier will be completed.

4.2 Study of FEL Saturation and Efficiency

A two-stage taper wiggler magnet will be constructed and a ~1 kW, 94 GHz driven tube will be procured. Together these will allow for studies of FEL saturation and efficiency enhancement at the ~400 kW output power level.

4.3 Design of a 5 MW FEL

The final design of a multimegawatt FEL amplifier will be completed and experimental preparations will be initiated.

APPENDIX A1

Calculation of Beam Resonance Energy

We may determine resonant axial velocity v_z first from the following FEL equations:

$$\omega = k_w v_z + k_{sz} v_z \tag{1}$$

$$\omega^2 = k_{sz}^2 c^2 + \omega_{cut}^2 \tag{2}$$

where ω is the wave frequency (fixed by EIO source), ω_{cut} is the cut-off frequency in the waveguide for the TE_{01} mode, and k_{sz} is the axial wavenumber of the wave in the waveguide.

For the TE_{01} mode we have $\omega_{cut} = \pi/b$ where b is the narrow waveguide dimension. Then from Eq. (2),

$$k_{sz} = \sqrt{(\frac{\omega}{c})^2 - (\frac{\pi}{b})^2}. \tag{3}$$

v_z is determined from Eq. (1) as

$$v_z = \frac{\omega}{(k_w + k_{sz})}; \tag{4}$$

i.e., v_z equals the phase velocity of the FEL pondermotive beat wave. We further consider beam velocity, v_x, yet neglect v_y.

From $v_x/v_z = a_w/\gamma$ we get

$$c^2 \left(1 - \frac{1}{\gamma^2}\right) = \left[1 + \left(\frac{a_w}{\gamma}\right)^2\right] v_z^2. \tag{5}$$

Then we may solve Eq. (5) for the resonance energy γ_r to obtain

$$\gamma_r = \left[\frac{1 + a_w^2 \frac{v_z^2}{c^2}}{1 - \frac{v_z^2}{c^2}}\right]^{1/2} \tag{6}$$

where $a_w = (e/mc)(B_\perp/k_w)$.

Using Eqs. (3), (4) and (6), values of resonance energy may be calculated for given values of the waveguide dimension b. Values of resonance kinetic energy vs. b are displayed in Table A1.

Table A.1. Resonance kinetic energy vs. waveguide height
(frequency = 94 GHz, wiggler field = 0.48 Tesla, wiggler period = 0.96 cm)

b (meter)	energy (keV)
0.00320	472.4
0.00310	491.8
0.00300	515.2
0.00290	544.3
0.00280	581.1
0.00270	629.5
0.00260	695.9
0.00250	793.0
0.00240	950.2
0.00230	1257.0

TASK B

THEORY AND MODELING OF HIGH FREQUENCY, HIGH POWER GYROTRON OPERATION

Executive Summary

A number of important issues in the development of high power gyrotrons center on the ability to predict and improve the performance of designs. These issues include the elimination of mode competition, the optimization of efficiency, the minimization of wall loading, and the elimination of mode conversion at various points in the cavity. Also included is the issue of beam quality which can strongly affect the operation of a device.

While existing tools have had some success in predicting device performance, there are still a number of unexplained experimental results. Included here are the relatively poor performance of the simple tapered cavities tested at the Massachusetts Institute of Technology, the unexpectedly low mode purity of the 110 Ghz Varian gyrotron at General Atomic Corporation, and the large velocity spreads observed in the beams produced by magnetron injection guns.

Our group has undertaken a theoretical study of these issues which we describe in the next section. Our main contribution has been the development of a multimode simulation code, MAGY, which has successfully predicted the occurrence of mode competition in the MIT simple tapered cavity experiments. The code was also used to design a simple tapered cavity which is be free of mode competition, and which operated at an efficiency almost twice that of the previous tapered cavity. This code can is also being used to determine the output mode purity of gyrotrons such as the one at GA. Additionally, our group has studied a number of other problems relevant to high power gyrotron research which we describe as well.

In summary, the design of high power gyrotrons for fusion applications requires a strong theoretical and modeling base. The efforts of our group are aimed at providing this base.

Contents

1 Introduction

A number of important issues in the development of high power gyrotrons center on the ability to predict and improve the performance of designs. These issues include the elimination of mode competition, the optimization of efficiency, the minimization of wall loading, and the elimination of mode conversion at various points in the cavity. Also included is the issue of beam quality which can strongly affect the operation of a device.

While existing tools have had some success in predicting device performance, there are still a number of unexplained experimental results. Included here are the relatively poor performance of the simple tapered cavities tested at the Massachusetts Institute of Technology, the unexpectedly low mode purity of the 110 Ghz Varian gyrotron at General Atomic Corporation, and the large velocity spreads observed in the beams produced by magnetron injection guns.

Our group has undertaken a theoretical study of these issues which we describe in the next section. Our main contribution has been the development of a multimode simulation code, MAGY, which has successfully predicted the occurrence of mode competition in the MIT simple tapered cavity experiments. The code was also used to design a simple tapered cavity which is be free of mode competition, and which operated at an efficiency almost twice that of the previous tapered cavity. This code can is also being used to determine the output mode purity of gyrotrons such as the one at GA. Additionally, our group has studied a number of other problems relevant to high power gyrotron research which we describe as well.

In summary, the design of high power gyrotrons for fusion applications requires a strong theoretical and modeling base. The efforts of our group are aimed at providing this base.

2.1 Nonlinear Simulation of High Power Gyrotrons

We have used our recently developed[1] nonlinear, self-consistent, time-dependent, multi-mode gyrotron simulation code (which we have named the MAGY code) to study the operation of a number of different gyrotron configurations. In the code, the radiation field is expressed as a superposition of TE_{lm} wave guide modes modulated by a time and axial distance dependent amplitude. The radiation field profile satisfies outgoing

boundary conditions at both ends of the simulation region. Included in the code are the effects of DC voltage depression, AC space charge calculated in the distributed beam approximation [2], and velocity and pitch angle spread for the incoming beam. The code has been bench marked against the single frequency steady state Fliflet code and agrees with that code in cases in which steady state single frequency operation is achieved.

2.1.1 Simulation of MIT *TE* 16,2 tapered cavity experiments

In support of the experimental effort at MIT we have simulated a series of tapered cavity experiments with varying lengths, L_c, and varying input taper angles, θ_{in}. These cavities are illustrated in Fig. 1.

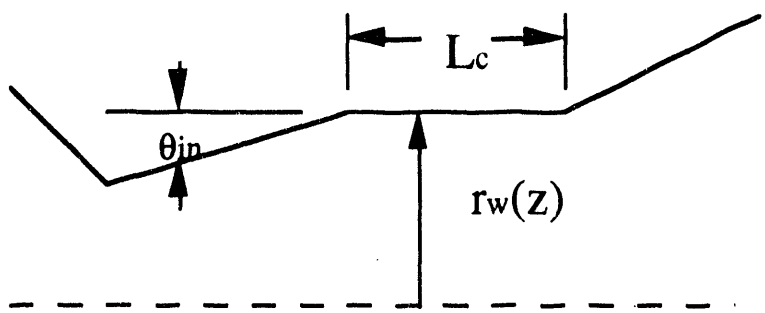

Figure 1. Tapered Cavity

The parameters for the three cavities are listed in Table 1

Table 1

Cavity	θ_{in}·	L_c	Q_{hot} [40 A]
MIT Short	1°	.5 cm.	422
Maryland Long	4°	1.1 cm.	776
Maryland Short	4°	.76 cm.	452

Measured and predicted efficiency versus beam current for the three cavities is displayed in fig. 2. The experiments were performed by the research team at MIT and results have been reported in refs. [3,4]. The results for the individual cavities will now be discussed separately.

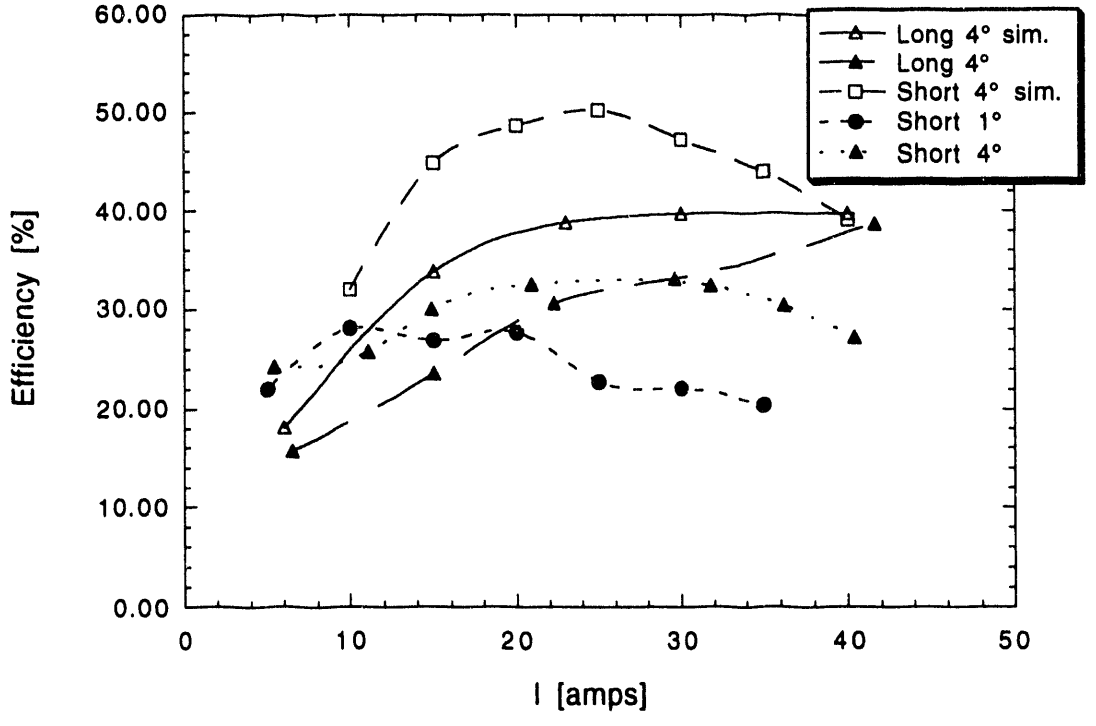

Figure 2. Efficiency versus beam current for three cavities. The results of simulation are indicated by open symbols

The first cavity (MIT Short 1 °) experienced mode competition involving the excitation of backward *TE* 15,2 modes in the throat of the cavity and subsequent excitation of *TE* 17,2 modes as a result of nonlinear mode beating. The simulations and measurements for this cavity were reported in ref. [4]. The predicted and measured frequencies for the various modes agreed well. Both the simulations and the experiments showed that the operating efficiency was well below that which would be expected on the basis of single mode theory. The simulations tended to give lower than measured efficiencies as is shown in fig. 3. where efficiency is plotted versus pitch angle for a current of 40 Amperes.

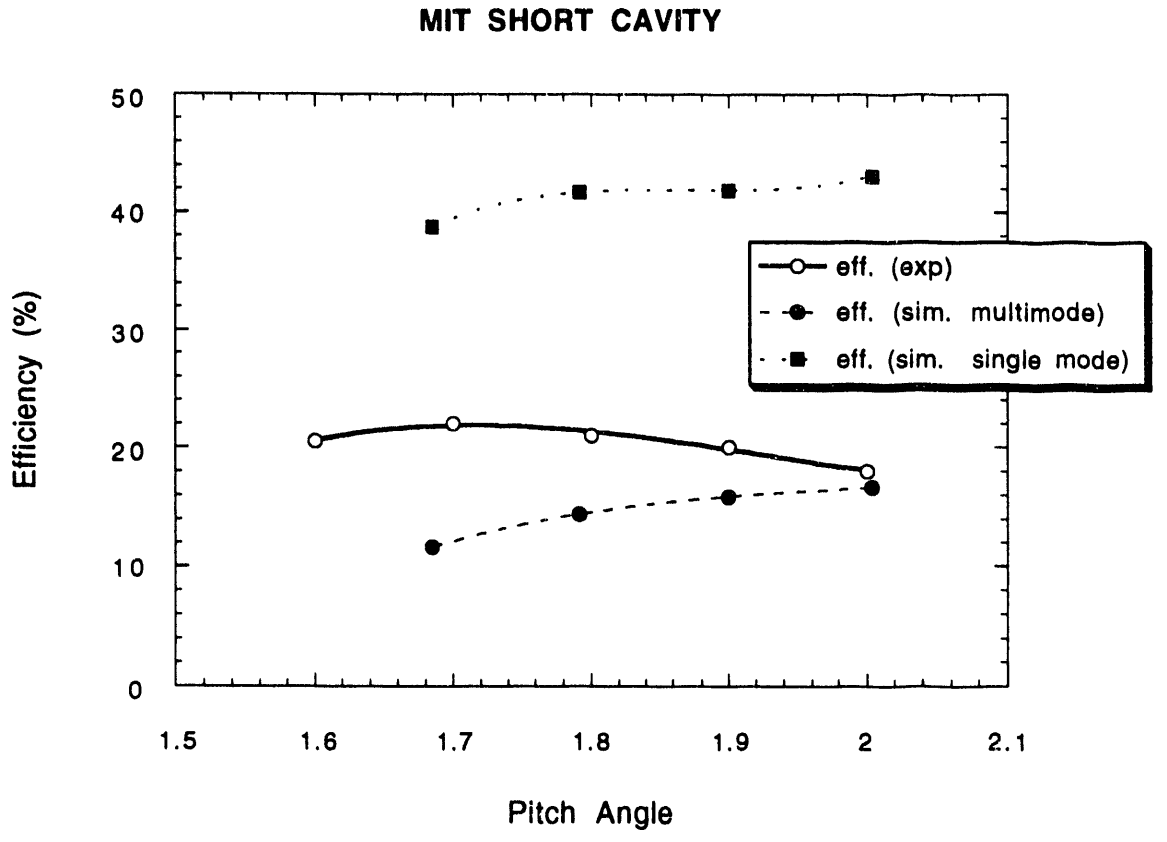

Figure 3 Efficiencies versus pitch angle for the MIT short cavity

To test whether mode competition was indeed responsible for the poor efficiency, a cavity with a larger input taper angle was designed and tested. This cavity (Maryland Long 4 °) was designed with a longer straight section so that efficiency would peak at lower values of the pitch α. As a result the cavity Q was raised. The experimental results for this cavity showed higher efficiency than the previous cavity (MIT Short). The maximum efficiency that was obtained was about 40% and the maximum output power was 1.3 MW. No mode competition was observed in either the simulation or the experiment. The predicted and measured efficiencies for the Maryland long cavity are shown in Fig. 4.

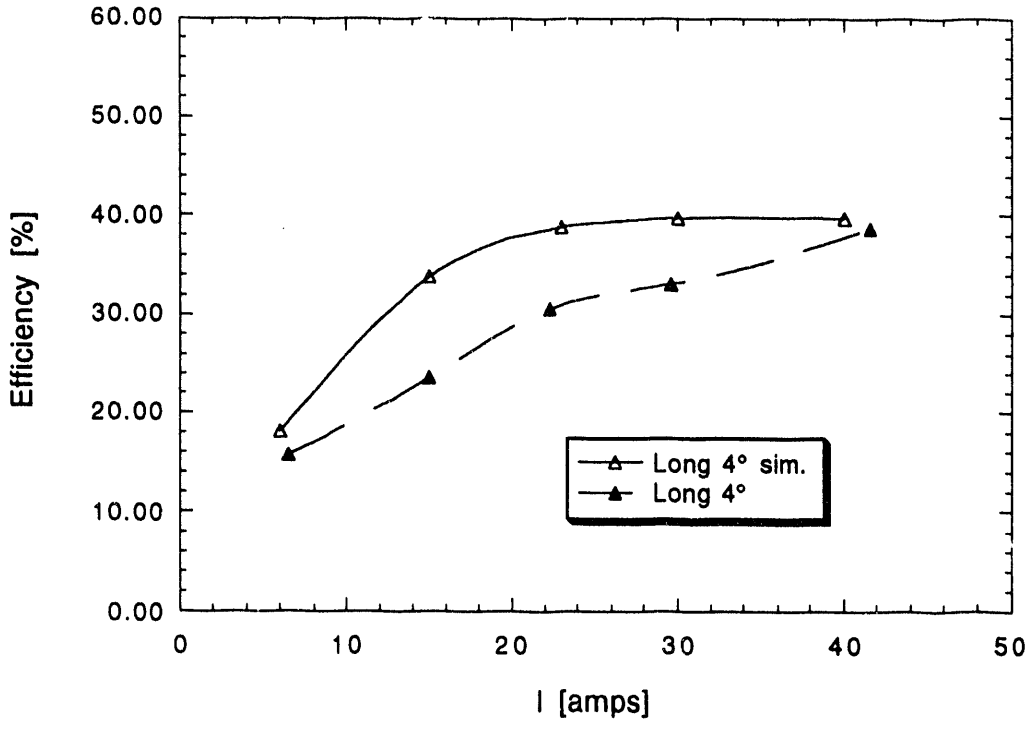

Figure 4. Efficiency versus current for the Maryland Long cavity

Notice that the efficiencies agree well only at the highest currents. Further, it was experimentally observed that the efficiency peaked at a pitch angle lower than what was predicted. Thus, there are indications that mode competition is not the sole cause of efficiency degradation in these tapered cavities.

This was further born out by the experiments conducted on the Maryland short 4 ° cavity. In this cavity, the straight section length was reduced so that the quality factor Q would be comparable to that of the MIT Short cavity. Plots of efficiency versus current for this cavity are shown in fig. 5.

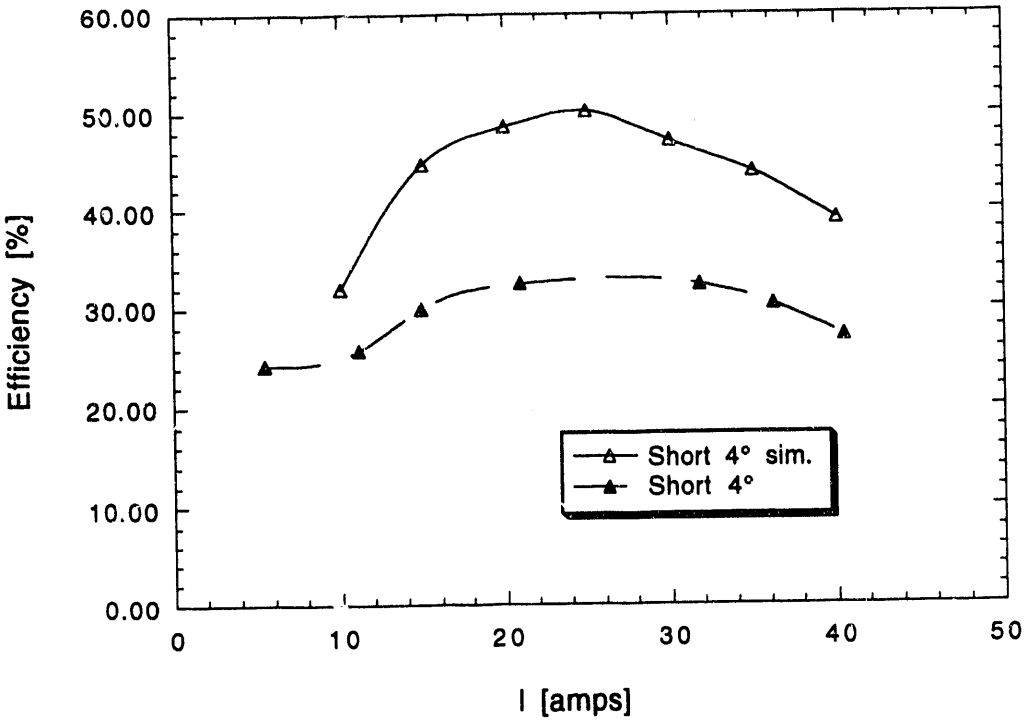

Figure 5. Efficiency versus current for the Maryland Short cavity.

Again, no mode competition was observed in this cavity in either the simulation or the experiments. While the efficiency is lower than expected, it is higher than that of the MIT short cavity which had a similar Q value, but a different input taper angle (See fig. 2). Thus, part of the efficiency degradation can be attributed to mode competition, while the remainder of the degradation is unexplained. A general conclusion from the current studies of simple tapered cavities is that longer cavities with steeper input angles seem to be preferable to shorter cavities with shallow input taper angles.

2.1.2 Simulation of the MIT two section cavity

Researchers at MIT have obtained high output power with a two section cavity as depicted in fig. 6.

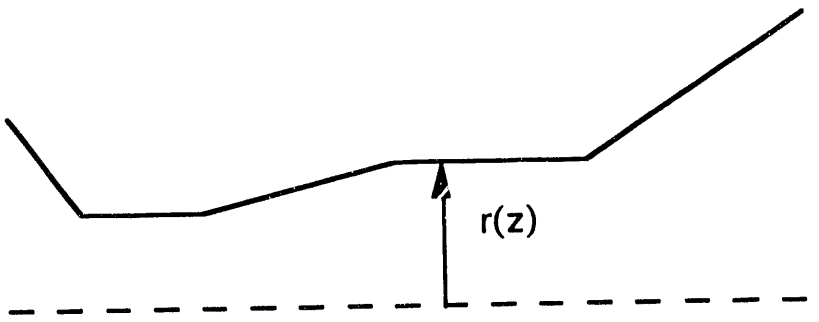

Figure 6. Wall radius for the two section cavity.

We have simulated the operation of this cavity with the time dependent code and results in the form of efficiency versus current are shown below in fig. 7. Experimental results were provided by Ken Kreischer.

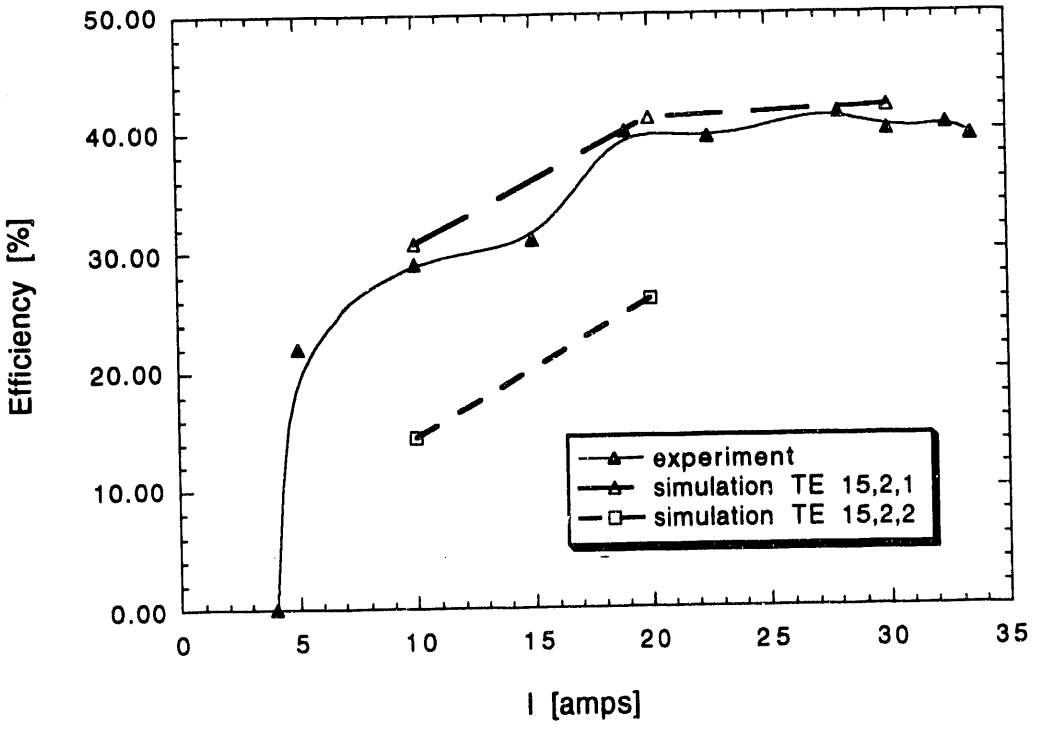

Figure 7. Efficiency versus current for the two section cavity

The simulated efficiency depends strongly on the shape of the RF field profile. Two different field profiles can be reached depending on the initial conditions of the simulation. One can obtain either a TE 15,2,2 mode or a TE 15,2,1 mode. This is illustrated below in figs. 8a and 8b.

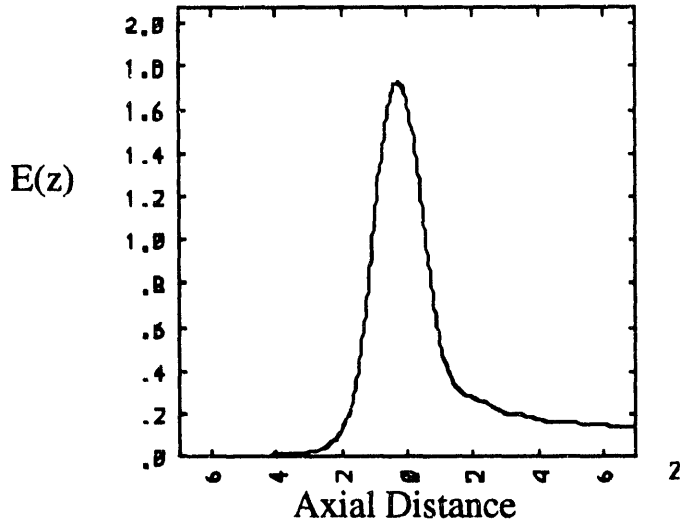

Figure 8a. Field profile for the TE 15,2,1 mode

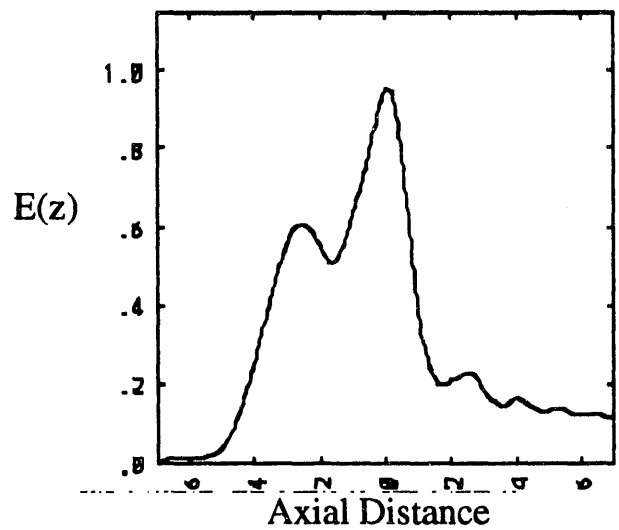

Figure 8b. Field profile for the TE 15,2,2 mode

The above simulations were obtained assuming only a single transverse mode (the TE 15,2) was present. We are now examining the transverse mode competition problem for this cavity as well as the role of the start up scenario in determining which longitudinal mode is reached.

2.1.3 Design of *TE* 22,5 high power cavity

We have conducted mode competition studies on a design for a tapered cavity operating at 110 GHz in the TE 22,5 mode. The cavity parameters

were chosen so as to eliminate mode competition of the type found in the short tapered cavity discussed above. The parameters for the design are listed in table 2.

Table 2. High Power Gyrotron Parameters

Beam Voltage	80 kV
Beam Current	50 A
Beam Pitch Ratio	1.6
Cavity Length	1.25 cm.
Cavity Radius	1.823 cm.
Input Taper Angle	3.52 °
Output Taper Angle	5.28 °
Magnetic Field	4.336 T
Efficiency	47 %
Output Power	1.86 MW
Maximum Wall Dissipation	1.16 kW/ cm^2

2.1.4 Simulation of mode conversion in a 110 GHz gyrotron

Recent measurements indicate that the power emerging from the Varian 110 GHz gyrotron at General Atomic Corporation contains a mixture of transverse modes rather than being the relatively pure *TE* 15,2 mode. We have begun a theoretical investigation of the excitation of other transverse modes in both the cavity and the down stream taper region of the cavity. Two processes that might lead to excitation of unwanted modes are mode conversion due to the non uniform wall radius and mode excitation by the bunched beam as it leaves the cavity. The first possibility is not likely since the cavity has been designed to minimize this process. Further, the observed mode purity depends on the magnetic field strength which implies that the excitation of the unwanted modes occurs through the electron beam in some way. This leads to a consideration of the second effect. We are currently in the process of modifying our simulation code to include the TM as well as TE modes which might be excited in the output taper of the cavity.

2.1.5 Simulation of proposed Varian high power gyrotron

At the request of Kevin Felch we have simulated a proposed 110 GHz TE 15,4 high power gyrotron. We have tested this design and found that it should operate in a single transverse mode.

2.1.6 Distribution of MAGY

We have traveled to Varian and installed our code MAGY on their work station. This code is currently being used in Varian's design efforts.

2.2 Linear and nonlinear studies of space charge instability in gyrotron beams

The efficiency of operation of gyrotron cavities is strongly degraded if the injected beam has an RMS energy spread as large as 10 %. It is commonly assumed that the beam emerging from a magnetron injection gun is monoenergetic. However, the presence of instabilities in the gun region would induce an energy spread in the electron beam. We have studied the linear and nonlinear theory of one such instability, the electrostatic cyclotron maser instability. This instability is convective in nature and its severity is measured by the number of spatial exponentiations a disturbance experiences in propagating from the gun to the cavity. Our studies have shown that this instability is strongly affected by the inhomogeneity of the magnetic field in the gun region. This inhomogeneity, coupled with a pitch angle spread on the beam, leads to stabilization of the instability. Shown below in fig. 9 is the profile of magnetic field for the MIT 140 GHz magnetron injection gun.

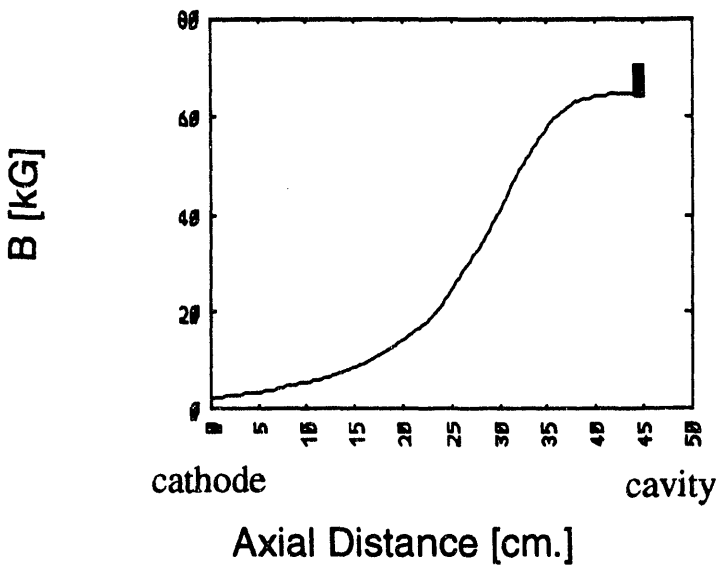

Figure 9. Profile of magnetic field versus axial distance for the MIT 140 GHz gyrotron.

The corresponding number of exponentiations (gain) for the instability on the beam in this profile is shown in fig. 10, below, as a function of frequency for several assumed values of the RMS spread in parallel velocity.

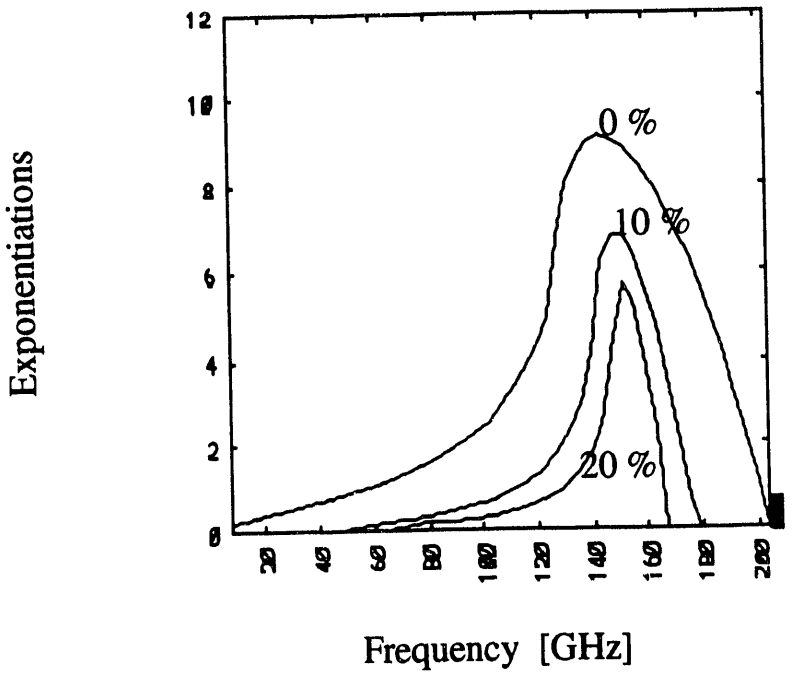

Figure 10. Number of spatial exponentiations versus frequency for beams with three different axial velocity spreads.

For a cold beam the number of spatial exponentiations is large enough for the instability to reach saturation and according to our nonlinear simulations induce an energy spread of about 9 % on the beam. However, the axial velocity spread of the beam has recently been measured by Guss. et al [5] and found to be significant, perhaps as large as 25 % . In this case, the instability would not have enough growth to reach saturation.

2.3 Studies of parametric mode interactions in harmonic gyrotrons

The typical type mode competition that is studied for gyrotron devices involves the interaction among modes which all have nearly the same

frequency, that is the cyclotron frequency. Another possible type interaction involves the competition among modes with widely different frequencies, for example, the competition among modes which are resonant with different cyclotron harmonics. In this case one can consider three wave parametric interactions in which three modes with frequencies ω_1, ω_2, and ω_3, and azimuthal mode indices m_1, m_2, and m_3, interact if the following matching conditions are satisfied,

$$\omega_1 + \omega_2 = \omega_3 \qquad \text{and} \qquad m_1 + m_2 = m_3.$$

We have studied both the general framework for interactions of this type [6] as well as investigated numerically the parameter regimes in which different forms of competition are possible [7]. We find that for certain parameter regimes, operation at the second harmonic is possible even if the current is above linear start current for the fundamental.

2.4 Nonlinear simulation of quasi-optical gyrotrons

2.4.1 Self consistent field calculations in QO resonators

The quasi-optical gyrotron interaction takes place in an open resonator. One issue which has never been addressed is the degree to which the electron beam modifies the field structure of the modes of the empty resonator. A related question is what is the distribution of output radiation that leaves the cavity. This later issue is important since the spatial distribution of the emerging radiation will affect the efficiency of coupling the output to a transmission system. To address these questions, we have, in collaboration with the group at the CRPP in Lausanne Switzerland, developed a three dimensional electromagnetic field solving code, which includes the self consistent effects of the electron beam and solves for the fields inside the quasi-optical resonator. The code was benchmarked against experiments [8] in which the electron beam was simulated by a dielectric tube. The presence of the tube lowered the quality factor of the cavity and this could be compared with simulations. Shown below in fig. 11. are results for the equivalent round trip transmission coefficient $T = \exp(-2\omega d/Qc)$ versus displacement of the tube along the axis of the cavity.

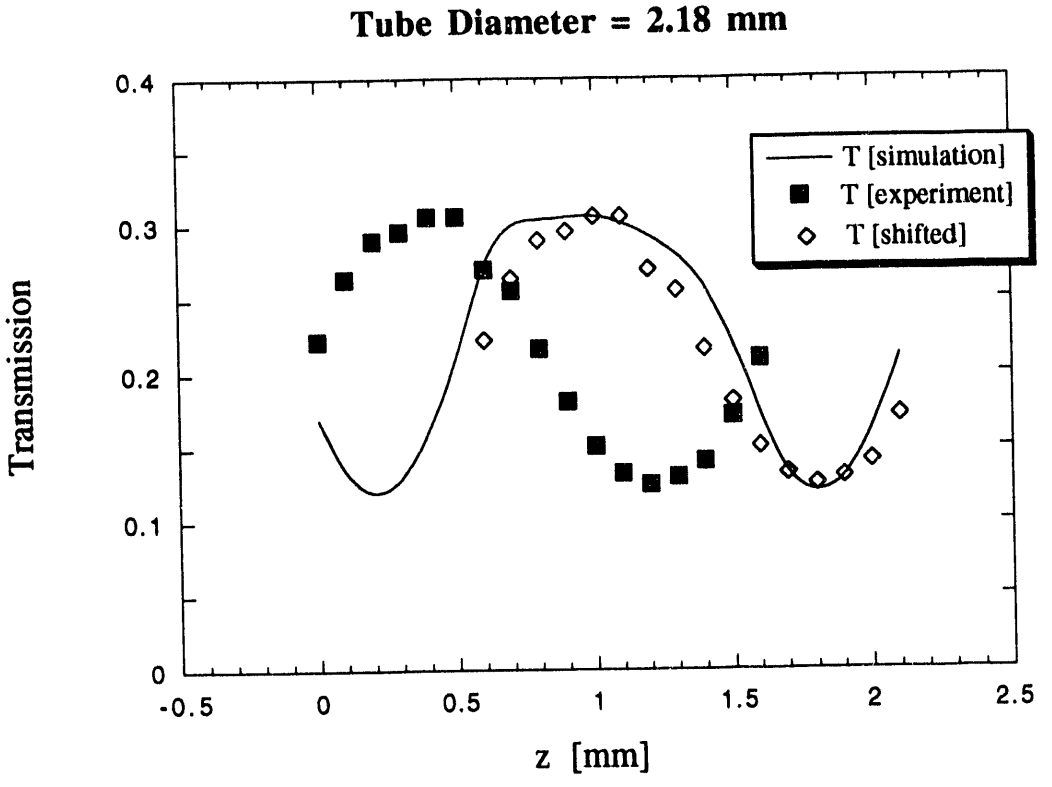

Figure 11. Effective transmission coefficient versus tube displacement.

The solid symbols are the experimental data, the curve is the result of the numerical simulation. In the experiment there is a large uncertainty in the absolute location of the tube. Shifting the experimental data by .6 mm leads to the open symbols which agree quite well with the simulation. Shown below in fig. 12 is a surface plot of the magnetic field on the surface of one of the mirrors for the case in which the radiation is excited by a beam of electrons.

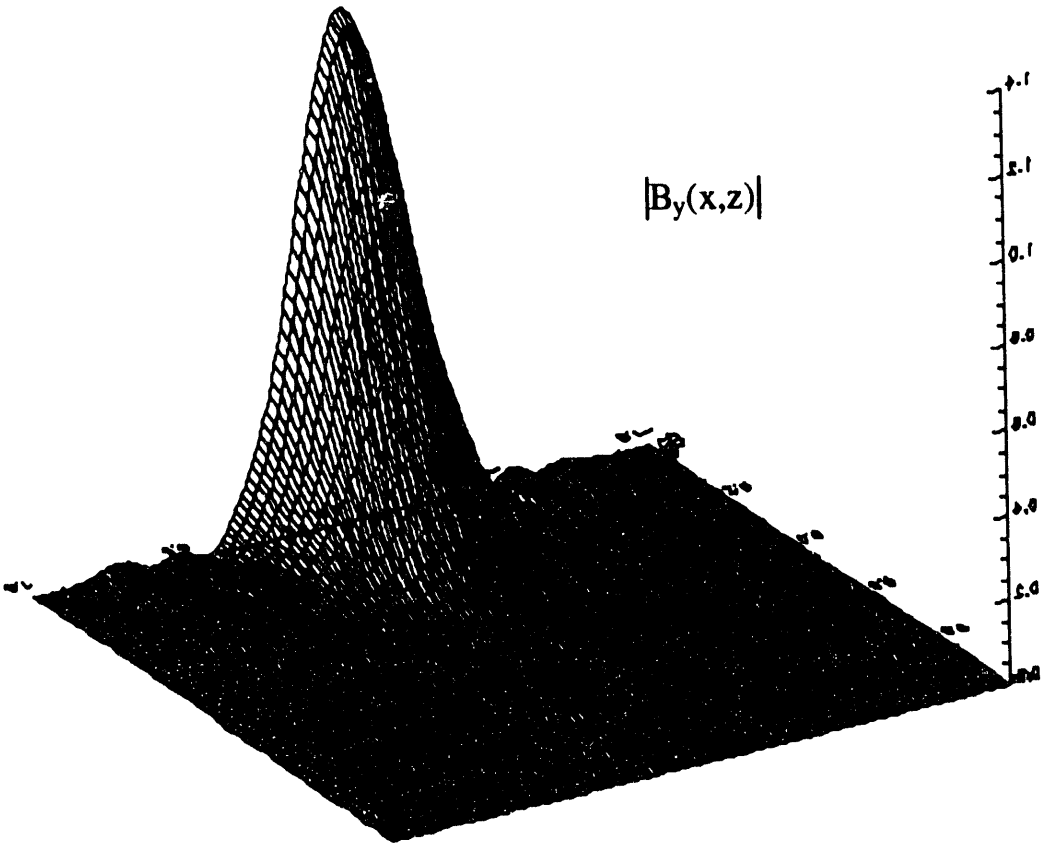

Figure 12. Magnetic field distribution of the surface of one of the mirrors in a quasi-optical gyrotron.

The simulation indicates that the field within the cavity is well approximated by a guassian mode and that the power emerging from a device in which one of the mirrors is a grating should be easily matched to a transmission system. Finally, the simulations seem to rule out the possibility that the poor efficiency which is observed in QO experiments is related to beam modification of the field structure in the interaction region.

2.4.2 Simulation of α priming in the NRL QO

Recent experiments at NRL have yield improved performance in terms of higher efficiency when the rise of the cathode voltage precedes by a small amount the rise of the main anode voltage [9]. This has been called α-priming because the beam pitch ratio, α, reaches a large value before the beam energy reaches its flat top value. Below are simulations and experimental results (provided by Rich Fischer and Arne Fliflet) for efficiency versus beam voltage.

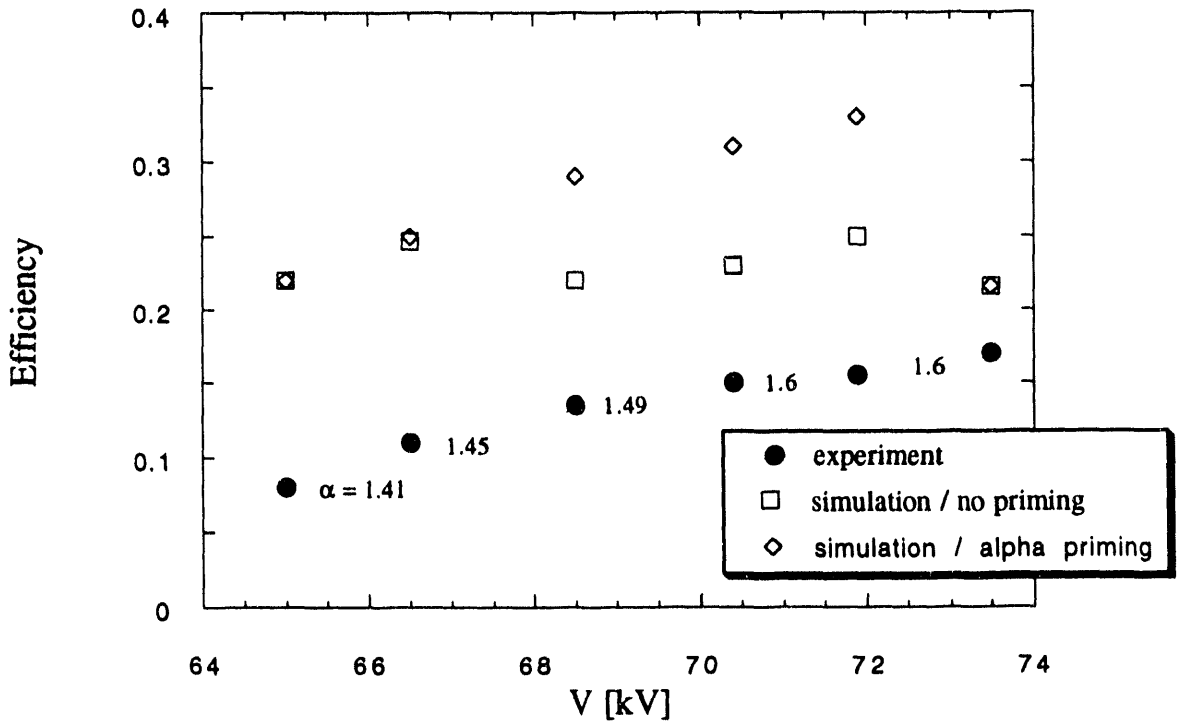

Figure 13. QO efficiency versus beam voltage.

The simulations show some dependence on whether or not the beam has been α-primed. As can be seen, however, the experimental efficiencies are still well below that predicted by the simulations. Thus, the cause of efficiency degradation in the experiments, as well as the role of α-priming in the experimental operation is not understood. Finally, we have made available our quasi-optical gyrotron simulation code to researchers at NRL.

References

1 S. Y. Cai, T. M. Antonsen, Jr. G. Saraph, and B. Levush, Int. J. Electron. **72** 759 (1992).

2 R. G. Kleva, T. M. Antonsen, Jr. and B. Levush, Phys. Fluids **31**, 375 (1988).

3 W. C. Guss, M. A. Basten, K. E. Kreischer, R. J. Temkin, T. M. Antonsen, Jr., S. Y. Cai, G. Saraph, and B. Levush, Phys. Rev. Lett. **69**, 3727 (1992).

4 W. C. Guss, M. A. Basten, K. E. Kreischer, R. J. Temkin, T. M. Antonsen, Jr., S. Y. Cai, G. Saraph, and B. Levush, Proceedings of the Seventeenth International Conference on Infrared and Millimeter Waves,Pasadena CA. SPIE Vol. 1929, R. J. Temkin Editor, 264 (1992).

5 W. C. Guss, T. L. Grimm, K. E. Kreischer, and R. J. Temkin, Proceedings of the Fifteenth International Conference on Infrared and MillimeterWaves,Orlando FL. SPIE Vol. 1514, R. J. Temkin Editor, 416 (1990).

6 G. S. Nusinovich, Int. J Electron. **72**, 795 (1992).

7 G. P. Saraph, G. S. Nusinivich, T. M. Antonsen, Jr. and B. Levush, Bull. Am. Phys. Soc. **37**, 1355 (1992).

8 T. M. Antonsen, Jr., A. Bondeson, M. Roulin, and M. Q. Tran Proceedings of the Seventeenth International Conference on Infrared and Millimeter Waves,Pasadena CA. SPIE Vol. 1929, R. J. Temkin Editor, 382 (1992).

9 R. P. Fischer, A. W. Fliflet, and W. M. Manheimer, Proceedings of the Seventeenth International Conference on Infrared and Millimeter Waves,Pasadena CA. SPIE Vol. 1929, R. J. Temkin Editor, 254 (1992).

3 STATEMENT OF WORK (TASK B)

3.1 Simulation of High Power Gyrotrons

We intend to continue our support of the experimental high power gyrotron effort by providing simulations and modeling of devices and experiments at MIT, Varian, and GA. Specific tasks include the following.

3.1.1 Simulation of mode conversion in a 110 GHz gyrotron

We will complete our efforts at determining the causes of mode impurity described in sec 2.1.4 for the 110 GHz gyrotron at General Atomic Corporation. We are currently modifying our simulation code to include both TE and TM modes in the interaction region and the output taper section. When completed, this code will include the two possible causes of mode excitation discussed in 2.1.4, mode conversion due to non uniform wall radius, and mode excitation by the bunching of the beam in the cavity. This latter effect depends on the profile of the magnetic field in the output taper section which we are in the process of obtaining from Varian.

3.1.2 Multi-frequency simulation of the MIT two section cavity experiment

We will continue our support of the experimental effort at MIT by completing multi-frequency simulations of the two section cavity described in sect. 2.1.2. The important issues are whether the two section cavity is stable with respect to parasitic modes and whether the time dependent start up conditions in a simulation lead to the excitation of the correct TE 15,2,1 mode. There is a fair amount of experimental data for this cavity which can be compared with the results of the simulations.

3.1.3 Simulation of the MIT 230-280 GHz experiments

Our preliminary simulations of these experiments have indicated that mode competition with backward waves of the form found in the 140 GHz experiments is prevalent. In order to make more detailed comparisons we will have to perform additional simulations for the exact experimental conditions.

3.1.4 Mode map for the 140 GHz experiment

Extensive data have been taken for the dependence of the operating mode on magnetic field strength in the MIT 140 GHz experiments described in sec. 2.1.1. We will attempt to reproduce these dependences in the form of a partial mode map. This is a computationally intensive effort since it has been found that a description of the mode competition in the 140 GHz experiments depends sensitively on both the assumed pitch angle spread as well as the distribution of pitch angles in the injected beam. Pursuit of this effort on a full time basis would slow down considerably our efforts in other areas.

3.1.5 Design of multi-megawatt 110 GHz gyrotrons

The new direction toward multi-megawatt gyrotrons requires considering devices with larger cavities in order that the peak density of power dissipated in the wall be kept at an acceptable level. These cavities will have a higher mode density and will have to be designed to be immune to mode competition. We will aid MIT in its efforts in designing this new generation of experiments.

3.2 Gyrotron Beam Quality

Experimental evidence indicates that the beam entering a gyrotron cavity contains a large spread in pitch angles, in contrast to the relatively cold beams which are predicted by simulation codes under the same conditions. Further, there is strong evidence that a significant population of trapped particles exists between the gun and the cavity. We will begin a theoretical effort to study the factors affecting the pitch angle distribution and lifetime of these particles and their influence on the quality of the beam entering the interaction cavity. Our initial efforts will be aimed at identifying important physical phenomena, quantifying their importance, and proposing experiments to test our understanding of the operation of magnetron injection guns. One of the first studies will aim at determining the life-time of trapped particles in the presence of symmetric fields. Second we will try to identify possible instability mechanisms that will modify the trapped particle population. An effort such as this should be coupled with an experiment, and we will pursue options for such an experiment both in the United States and abroad.

3.3 Mode competition in harmonic gyrotrons

We intend to complete our studies of competition among harmonics in gyrotrons. This work is undertaken as part of the PhD dissertation of one of the students supported by the grant. The next step in our studies will be

to incorporate in MAGY the possibility of studying the interaction of modes at different cyclotron harmonics.

3.4 Nonlinear simulation of quasi-optical gyrotrons

One of the most important questions facing this approach concerns the means by which power is coupled out of the cavity in a form which is suitable for transmission to the plasma. The team of researchers at the CRPP in Lausanne Switzerland have developed an output grating which acts as a partially transmitting mirror. Our recently developed self-consistent field structure code described in sec. 2.4.1 treats this grating as a partially transmitting mirror. We propose to modify the code to include a more realistic description of the grating. This will allow the code to calculate precisely the expected purity (that is the degree to which the radiation can be considered a guassian beam.) of the output radiation.

END

DATE FILMED

6/17/93